This article has been accepted for publication in a future issue of this journal, but has not been fully edited. Content may change prior to final publication. Citation information: DOI 10.1109/LAWP.2019.2938872, IEEE Antennas and Wireless Propagation Letters

A Circular Beam-steering Antenna with Parasitic Water Reflectors

Lei Xing, *Member, IEEE*, Jiajia Zhu, Qian Xu, *Member, IEEE*, Dandan Yan, Yongjiu Zhao

***Abstract*—A salty water antenna with beam-steering characteristics is proposed. The antenna combines the idea of the electronically steerable parasitic array radiator (ESPAR) antenna and the water antenna to realize a 360° beam steering. The unique features of water antennas such as transparency, reconfigurability and liquidity are fully utilized. Both the computer simulations and measurements are conducted to validate the performance. The proposed design has a frequency range from 334 MHz to 488 MHz (S_{11} < -10 dB), high radiation efficiency (> 60%), 13 different working states and a maximum gain of 5.8 dB. Compared with existing pattern reconfigurable liquid antennas, this new antenna has a wider bandwidth, more working states and better invisible ability. It is therefore a promising candidate for a range of VHF or UHF applications, such as internet of things (IoT) and maritime applications.**

***Index Terms*—Electronically steerable parasitic array radiator (ESPAR) antenna, water antenna, pattern reconfigurable antenna.**

I. Introduction

LIQUID antennas are a new type of antennas with a range of attractive features [1-5]. Reconfigurable liquid antennas may be the most popular one, especially reconfigurable salty water antennas. They utilize unique features of salty water (liquidity, conformability, transparency, low cost and readily available in a maritime environment) and provide alternative ways of reconfigurations different from existing reconfigurable antennas [6-8]. Interesting reconfigurable salty water antennas were recorded, such as a broadband frequency reconfigurable salty water antenna [9], a high efficiency sea water monopole antenna [10], a metal loaded sea water antenna [11] and a frequency and pattern reconfigurable salty water antenna [12]. In the existing reconfigurable liquid antenna designs, frequency tunable liquid antennas are most frequently investigated [9-11], which offer various states in one structure. Pattern and polarization reconfigurable designs have less working states (usually 2 to 4 different states), which is limited for some applications [12-14].

To increase working states of reconfigurable antennas, electronically steerable parasitic array radiator (ESPAR) antennas could be a good candidate. This type of antennas consists of one driven element and several parasitic elements. Different radiation patterns can be generated by adjusting loads at the terminals of parasitic elements. No phase shifters and feeding networks are required, which reduces the complexity of the antenna design. Some designs based on ESPAR technology were reported including a 360° beam steering substrate integrated waveguide horn antenna [15], a compact antenna with reconfigurable pattern and polarization [16], an ESPAR antenna used for 2D direction of arrival estimation [17] and a liquid metal antenna with a 360° beam scanning range [18].

In this letter, a salty water antenna with circular beam-steering characteristics is proposed. Mechanical switches are integrated, which takes fully advantages of liquid's unique features. The proposed design has the following advantages:

1) The design combines the idea of the ESPAR antenna and the water antenna to realize 13 stable working states (1 omni-directional pattern and 12 directional patterns) in one simple structure without using extra phase shifter or feeding network.

2) A liquid control system is developed which controls the fluid effectively and efficiently in a general way. The system can be applied to other liquid antennas or antenna arrays.

3) The antenna can be totally turned off or drained when not in use, which is difficult to realize using metal.

4) Compared with liquid metals or organic liquids, the salty water used in the design is low cost, readily accessible and eco-friendly.

The letter is organized as follows. Section II introduces the antenna structure, the operation principle and the design of parasitic monopoles. Section III focuses on the fabrication and measurements of the water antenna. Section IV concludes the letter.

II. Antenna Configuration and Design

A. Antenna Configuration

The configuration of the proposed antenna is shown in Fig. 1. It consists of a circular ground plane, a driven monopole and 12 parasitic monopoles. The ground plane has a radius of R_{GND}. The driven monopole contains a water cylinder with a height of H_{DM}, a circular Teflon dielectric layer ($\varepsilon_r \approx 2.1$) with a radius of R_D and a height of H_D, and a top loaded copper disk with a radius of R_{TP}. Parasitic water monopoles with a height of H_{PM} are circularly distributed around the driven monopole with a distance of D_{PM} and a rotation angle of α_R. The number of

This work was supported in part by the National Natural Science Foundation of China (61601219 and 61701224) and Nature Science Foundation of Jiangsu Province (BK20160804).

L. Xing, J. Zhu, Q. Xu, D. Yan, Y. Zhao are with College of Electronic and Information Engineering, Nanjing University of Aeronautics and Astronautics, Nanjing, 211106, China (e-mail: emxinglei@foxmail.com).

This article has been accepted for publication in a future issue of this journal, but has not been fully edited. Content may change prior to final publication. Citation information: DOI 10.1109/LAWP.2019.2938872, IEEE Antennas and Wireless Propagation Letters

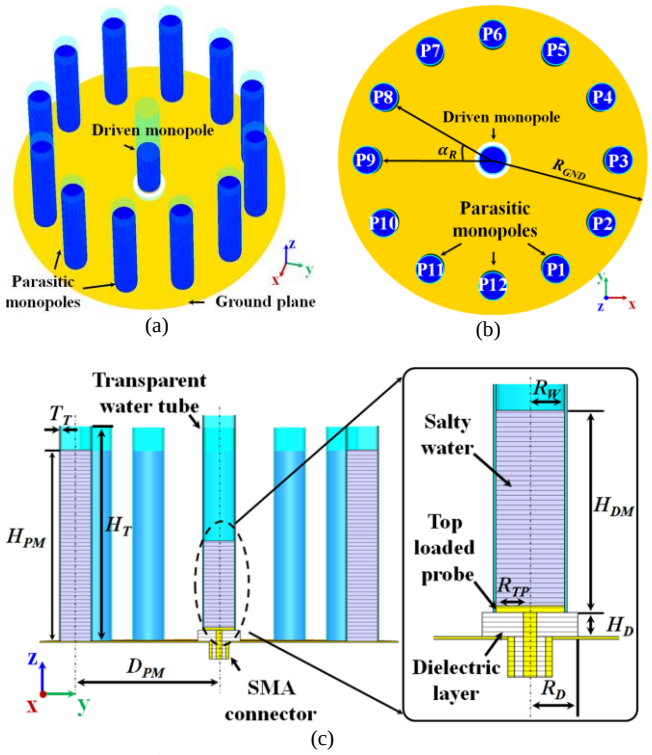

Fig. 1. Geometry of the proposed antenna. (a) Perspective view. (b) Top view. (c) Cross-section view.

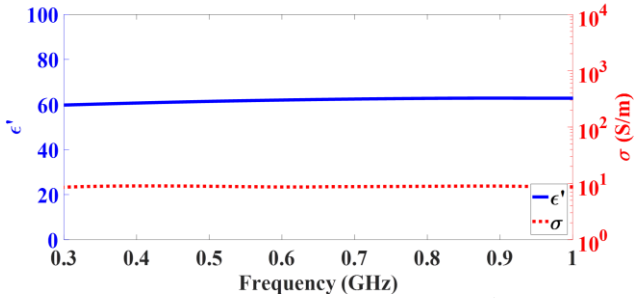

Fig. 2. The measured relative permittivity and conductivity of the salty water with salinity of 50 ppt at room temperature 25℃.

parasitic tubes $N_{PT} = 360^0/\alpha_R$ (N_{PT} = 12, $\alpha_R = 30^0$ in this design, and P1 to P12 represent parasitic tubes).

To simplify the design and fabrication, identical acrylic plastic transparent tubes ($\varepsilon_r \approx 2.7$) are used with inner radius R_W, thickness T_T and height H_T. A SMA connector is connected to the top loaded disk to feed the driven monopole antenna.

The salty water with salinity of 50 ppt (part per thousand) was used in measurements and simulations. The relative permittivity and conductivity of the salty water at room temperature (25℃) were measured using Agilent Dielectric Probe 85070 and the results are given in Fig. 2. It can be seen that the electric properties of the salty water with salinity of 50 ppt are quite stable across the frequency of interest.

B. Operation Principle

This design utilizes a movable reflector to realize pattern reconfiguration. When only the driven monopole is excited, the antenna has an omni-directional radiation pattern (state 1 in Fig. 3). When the driven and parasitic monopoles are excited, water-filled parasitic monopoles are coupled and work as reflectors. By configuring the adjacent water-filled parasitic

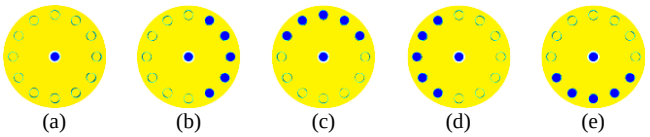

Fig. 3. Typical reconfigurations for the proposed design.

monopoles as a reflector, the proposed design is able to generate a directive pattern in an expected direction. Circularly shifting the configuration of working parasitic monopoles can steer the beam with a coverage of 360°. 13 states including 1 omni-directional and 12 directional patterns can be obtained and some typical states are shown in Fig. 3.

The attractive feature of using water monopoles is that both the water height and activating status can be dynamically tuned (*e.g.* microfluidic techniques), which has a higher degree of design flexibility than metal antennas. More importantly, the antenna can be totally "turned off" when not in use.

C. Parasitic Monopoles Design

The high gain response is desired for the proposed design, which can be achieved by tuning the value of the D_{PM}. The D_{PM} affects the phase consistency between the parasitic elements and the driven element, hence the gain of the proposed design. In this section, the effects of the D_{PM} are studied. For simplicity, the reconfiguration state in Fig. 3(b) and the spherical coordinates (r, θ, φ) are employed for the analysis.

The simulated phases of the far-zone electric field generated by the driven element and working parasitic elements in the azimuth plane as a function of D_{PM} are presented in Fig. 4 (The phases are obtained from analytical derivations [19] and numerical simulations). As the D_{PM} is increased from 180 mm to 240 mm, the phase generated by parasitic elements (P1 to P5) approaches to that of the driven element at $\varphi = 180^o$ (the direction of maximum gain). A directional pattern and a high gain can be acquired. When the D_{PM} is further increased, the phase of parasitic elements (P1 to P5) departs from that of the driven element, decreasing the total radiated field and deteriorating the gain. By fine tuning the value of the D_{PM}, a good phase consistency can be obtained when D_{PM} = 240 mm, resulting in a high total radiated field and a high gain. The simulated realized gains in the azimuth plane at 433 MHz are plotted in Fig. 5. It is observed that the maximum realized gain is gained at D_{PM} = 240 mm, which agrees with the phase analysis in Fig. 4.

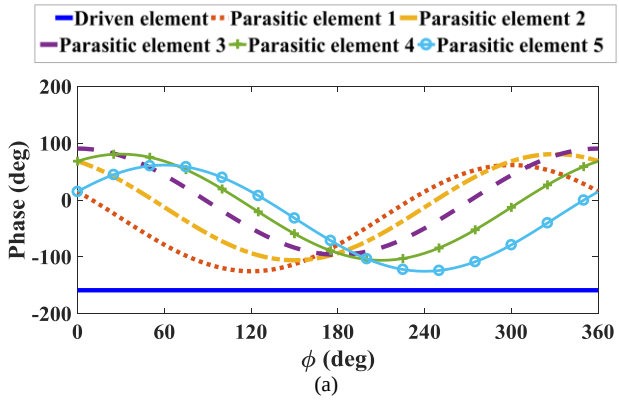

This article has been accepted for publication in a future issue of this journal, but has not been fully edited. Content may change prior to final publication. Citation information: DOI 10.1109/LAWP.2019.2938872, IEEE Antennas and Wireless Propagation Letters

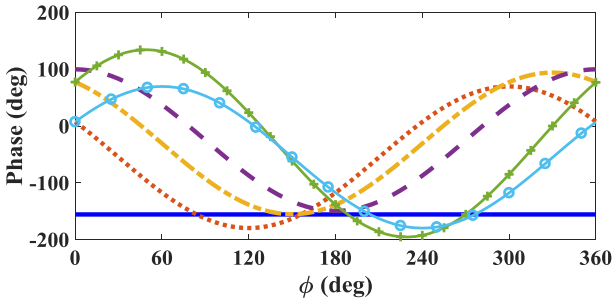

(b)

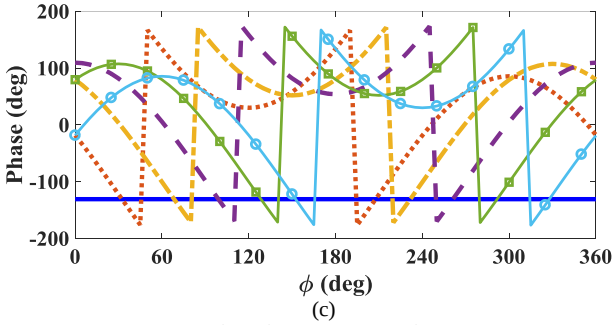

(c)

Fig. 4. Simulated phases of the far-zone electric field generated by the driven element and working parasitic elements for different values of D_{PM} in the azimuth plane ($\theta = 90^o, \varphi$ varies) at 433 MHz: (a) D_{PM} = 180 mm, (b) D_{PM} = 240 mm, (c) D_{PM} = 400 mm.

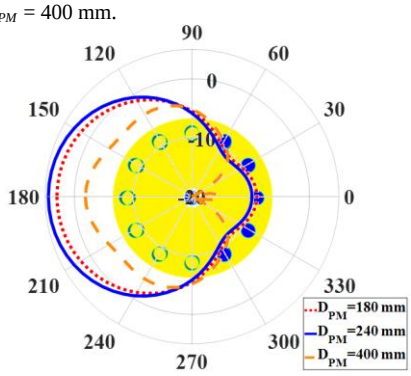

Fig. 5. Simulated realized gains (dB) in the azimuth plane ($\theta = 90^o, \varphi$ varies) with different values of D_{PM} at 433 MHz.

III. Antenna Fabrication and Measurements

To verify the design, the antenna with optimized dimensions was fabricated and the prototype is shown in Fig. 6(a). The optimal parameters are R_{GND} = 300 mm, α_R = 30°, H_T = 320 mm, T_T = 2 mm, R_W = 23 mm, H_{DM} = 130 mm, H_D = 18 mm, R_D = 33 mm, R_{TP} = 23 mm, H_{PM} = 320 mm, D_{PM} = 240 mm.

In this design, pattern reconfiguration is achieved by using microfluidic control system. A micropump with dimensions of 59 × 24 × 24 mm^3 and a weight of 40 g is utilized. The flow rate of the micropump changes linearly with voltage, from 240 mL/min to 400 mL/min. Mini-valves panel as shown in Fig. 6(c) are chosen to assist the injection and draining of the water. Acrylic connectors are fixed at the bottom of the water monopole to work as water inlets and outlets. Transparent water pipes are positioned underneath the ground plane to link the water monopoles and valves. Each water monopole has a corresponding valve and all the valves are allocated in the valves panel. As the pump is turned on, the distilled water is sucked from the reservoir and injected into the antenna through

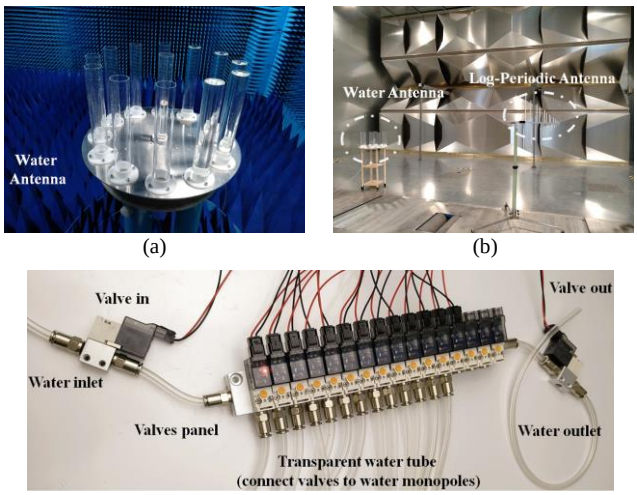

(a) (b) (c)

Fig. 6. (a) The proposed antenna in the anechoic chamber. (b) Reverberation chamber setup for the antenna efficiency test. (c) Enlarged view of the microfluidic control panel.

the acrylic connectors. When the water holder is filled to the desired level, the pump is turned off and all the valves are kept closed. By controlling the on and off states of valves, different working states of the antenna can be achieved, resulting in a pattern reconfiguration in this proposed design.

The S_{11}, radiation pattern, and realized gain were measured in an anechoic chamber, and the efficiencies were measured in a reverberation chamber (RC) [20], as shown in Fig. 6(a) and (b), respectively.

The simulated and measured S_{11}, radiation efficiency, and realized gain are compared in Fig. 7. It is evident that the proposed design has a bandwidth from 334 MHz to 488 MHz for S_{11} < -10 dB, which is slightly wider than the simulated bandwidth from 356 MHz to 455 MHz. The measured efficiency of the proposed design is higher than 60% across the working band, which is slightly lower than simulations. This is due to the deviation of the material losses considered in simulations. The maximum realized gain in the azimuth plane was measured. As a reference, the simulated maximum gain (a function of frequency) is added. The discrepancies between the simulations and measurements are mainly caused by three reasons: 1) the material difference; 2) the measurement environment uncertainties; 3) the reference antenna uncertainties. Overall, good agreement is obtained.

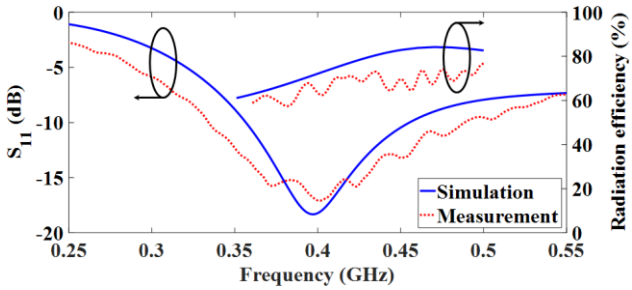

(a)

This article has been accepted for publication in a future issue of this journal, but has not been fully edited. Content may change prior to final publication. Citation information: DOI 10.1109/LAWP.2019.2938872, IEEE Antennas and Wireless Propagation Letters

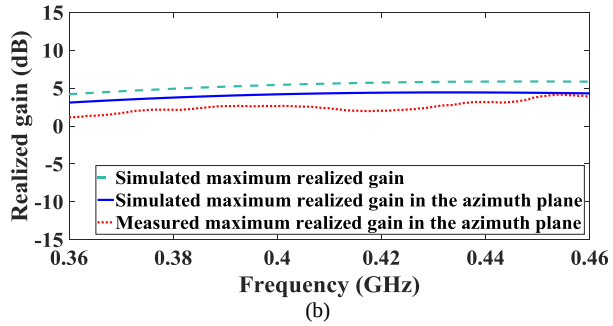

(b)

Fig. 7. Simulated and measured result comparison of the proposed design: (a) S_{11} (dB) and radiation efficiency; (b) realized gain.

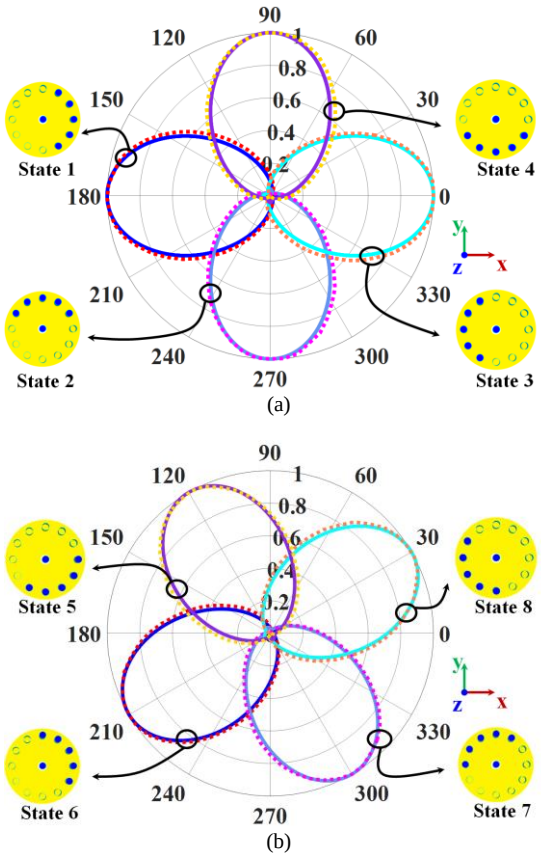

Fig. 8. Simulated and measured directional radiation patterns of the proposed design in the azimuth plane at 433 MHz with different working states: (a) State 1 - State 4; (b) State 5 - State 8; (c) State 9 - State 12.

TABLE I
COMPARISON OF THE PROPOSED DESIGN AND RELATED DESIGNS

Ref.	Fractional bandwidth (%)	Realized gain (dB)	Number of working states
[12]	78.7	-2 - 4	4
[13]	35.5	3 - 6	2
[14]	0.7	4.1- 4.5	3
This work	**37.4**	**4.2 - 5.8**	**13**

The radiation patterns in the azimuth plane corresponding to different states at 433 MHz are plotted in Fig. 8 (As the cross-polarization of the monopole antenna is very small, only the co-polarization is shown). By activating or deactivating parasitic monopoles, 12 stable directional radiation patterns can be obtained (the omni-directional pattern of the monopole antenna is well known and is not presented), which successfully demonstrate the pattern reconfigurability of the design.

A comparison between our design and related designs is given in Table I. It is apparent that this work provides more working states, higher realized gain and wider fractional bandwidth than most of pattern reconfigurable liquid antenna designs.

IV. Conclusions

In this letter, a radiation pattern reconfigurable salty water antenna has been proposed. It implements the ESPAR technology in the water antenna design and utilizes unique features of water such as the liquidity, the transparency and the design flexibility to realize a tunable water reflector and reconfigure the radiation pattern dynamically. The critical parameter of the proposed design has been studied, measurements have been conducted and the results agree well with simulations. A liquid control system is developed which manage the fluid effectively and efficiently in a general way, and can be applied for other liquid antennas.

It has been demonstrated that this antenna covers a frequency tuning range from 334 MHz to 488 MHz and has high radiation efficiency (> 60%) and a maximum realized gain of 5.8 dB. The radiation pattern can be tuned from omni-directional to directional with 13 different working states. More importantly, the antenna can be tuned to appear and disappear, which is difficult to realize using metal. This work successfully demonstrates the good performance and unique features of liquid antennas and provides a valuable reference for future liquid antenna designs.

Acknowledgment

The authors would like to thank Rongce Testing Technology Ltd (Nanjing, China) for the support of the measurements in a reverberation chamber.

References

[1] A. T. Mobashsher, A. Abbosh, "Reconfigurable water-substrate based antennas with temperature control," *Appl. Phys. Lett.*, 110, 253503, 2017.

[2] M. Wang, C. Trlica, M. R. Khan, M. D. Dickey and J. J. Adams, "A reconfigurable liquid metal antenna driven by electrochemically controlled capillarity," *J. Appl. Phys.*, 117, 194901, 2015.

[3] C. B. Fortuny, K. F. Tong, A. A. Armaghany, K. K. Wong, "A low cost fluid switch for frequency reconfigurable vivaldi antenna," *IEEE Antennas Wireless Propag. Lett.*, vol. 16, pp. 3151-3154, Nov. 2017.
[4] M. Zou, Z. Hu, C. Hua, and Z. Shen, "Liquid antennas," *in Wiley Encyclopedia Electrical and Electronics Engineering*, Hoboken, NJ, USA: Wiley, Nov. 2016.
[5] S. G. O'Keefe, S. P. Kingsley, "Tunability of liquid dielectric resonator antennas," *IEEE Antennas Wireless Propag. Lett.*, vol. 6, pp. 533-536, 2007.
[6] A. Raaza, S. Venugopalan, A. Mehta, "A novel 45 degree beam steerable antenna for modern communications," in *Proc. IEEE Sarnoff Symposium*, Princeton, New Jersey, USA, 2008, pp. 1-4.
[7] M. N. Jazi, T. A. Denidni, "Agile radiation-pattern antenna based on active cylindrical frequency selective surfaces," *IEEE Antennas Wireless Propag. Lett.*, vol. 9, pp. 387-388, Apr. 2010.
[8] Z. P. Wang, P. S. Hall, J. R. Kelly, and P. Gardner, "Wideband frequency domain and space domain reconfigurable circular antenna array," *IEEE Trans. Antennas and Propag.*, vol. 65, no. 10, pp. 5179–5189, Oct. 2017.
[9] H. Fayad, P. Record, "Broadband liquid antenna," *Electron. Lett.*, vol. 42, no. 3, pp. 133-134, 2006.
[10] C. Hua, Z. Shen, and J. Lu, "High-efficiency sea-water monopole antenna for maritime wireless communications," *IEEE Trans. Antennas Propag.*, vol. 62, no. 12, pp. 5968-5973, Dec. 2014.
[11] Z. Peng, X. Liang, W. Zhu, J. Geng, C. He, Y. Yao, Y. Qian, R. Jin, "Metal-loaded seawater antenna with high radiation efficiency and wideband characteristics," *IEEE Antennas Wireless Propag. Lett.*, vol. 16, pp. 1671-1674, 2017.
[12] R. Fan, Y. H. Qian, Q. X. Chu, "Frequency and pattern reconfigurable saline-water antenna array," *Microw. Opt. Technol. Lett.*, vol. 59, no. 9, pp. 2284-2289, 2017.
[13] Z. Chen and H. Wong, "Wideband glass and liquid cylindrical dielectric resonator antenna for pattern reconfigurable design," IEEE *Trans. Antennas Propag.*, vol. 65, no. 5, pp. 2157-2164, May 2017.
[14] J. J. Liang, G. L. Huang, K. W. Qian, S. L. Zhang and T. Yuan, "An azimuth-pattern reconfigurable antenna based on water grating reflector," *IEEE Access*, vol. 6, pp. 34804-34811, 2017.
[15] L. Ge, K. M. Luk and S. Chen, "360º beam-steering reconfigurable wideband substrate integrated waveguide horn antenna," *IEEE Trans. Antennas Propag.*, vol. 64, no. 12, pp. 5005-5011, Dec. 2016.
[16] C. Gu, H. Liu, T. H. Loh, M. Sobhy, J. Li, G. Wei, J. Xu, F. Qin, B. S. Izquierdo, R. A. A. Alhameed, "Compact smart antenna with electronic beam-switching and reconfigurable polarizations," *IEEE Trans. Antennas Propag.*, vol. 63, no. 12, pp. 5325-5333, Dec. 2015.
[17] L. Kulas, "Simple 2-D directional of arrival estimation using an ESPAR antenna," *IEEE Antennas Wireless Propag. Lett.*, vol. 16, pp. 2513-2516, 2017.
[18] J. R. Kelly and M. A. Tanha, "Reconfigurable 26 GHz liquid metal antenna capable of low loss continuous beam steering," in *Proc. IEEE Conference on Antenna Measurements & Applications (CAMA)*, Vasteras, Sweden, 2018, pp. 1-2.
[19] C. A. Balanis, Antenna Theory: Analysis and Design, Wiley, 2016.
[20] Q. Xu, Y. Huang, Anechoic and Reverberation Chambers: Theory, Design and Measurements, Wiley-IEEE, 2019.